

CrystEngComm

Accepted Manuscript



This is an *Accepted Manuscript*, which has been through the Royal Society of Chemistry peer review process and has been accepted for publication.

Accepted Manuscripts are published online shortly after acceptance, before technical editing, formatting and proof reading. Using this free service, authors can make their results available to the community, in citable form, before we publish the edited article. We will replace this *Accepted Manuscript* with the edited and formatted *Advance Article* as soon as it is available.

You can find more information about *Accepted Manuscripts* in the [Information for Authors](#).

Please note that technical editing may introduce minor changes to the text and/or graphics, which may alter content. The journal's standard [Terms & Conditions](#) and the [Ethical guidelines](#) still apply. In no event shall the Royal Society of Chemistry be held responsible for any errors or omissions in this *Accepted Manuscript* or any consequences arising from the use of any information it contains.



Hierarchical ZnO hollow microspheres with exposed (001) facets as a promising catalyst for the thermal decomposition of ammonium perchlorate

Received 00th January 20xx,
Accepted 00th January 20xx

DOI: 10.1039/x0xx00000x

www.rsc.org/

Shouqin Tian,^{*a} Neng Li,^a Dawen Zeng,^{*b} Haitao Li,^b Gen Tang,^c Aimin Pang,^c Changsheng Xie^b and Xiujian Zhao^a

Hierarchical porous ZnO hollow microspheres assembled by nanorods with exposed (001) facets on their external surface were one-pot prepared by a simple low-temperature wet chemical method without templates. The formation mechanism based on the chemical self-transformation was proposed. Importantly, these ZnO hollow microspheres exhibited a better catalytic activity for the thermal decomposition of ammonium perchlorate (AP) in lowering its decomposition temperature from 409 °C to 308 °C and decreasing its activation energy from 150 ± 14 kJ/mol to 63 ± 7 kJ/mol than the ZnO dispersed nanorods. This is attributed to the hierarchical porous structure with larger surface area and exposed (001) facets dominant on the external surface, which can facilitate the adsorption of HClO₄ and NH₃ gases from AP and the formation of active oxygen. The active oxygen will promote the oxidation reaction of NH₃ more completely in AP decomposition, thus leading to a significant decrease in the decomposition temperature and activation energy. Therefore, this work could provide a new insight into the thermal decomposition mechanism of AP as catalyzed by hierarchical micro/nano structures of metal oxides.

Introduction

Ammonium perchlorate (AP) is the most widely used oxidant in composite solid rocket propellant, generally accounting for 60%–90% of the total mass of the propellant, and its thermal decomposition process puts a great impact on the combustion performance of the propellant.¹ Several significant parameters for the thermal decomposition of AP, such as activation energy, the rate, and temperature of high-temperature decomposition (HTD), have a close relationship with the combustion performance of solid propellant, especially the burning rate. The lower the HTD temperature is, the shorter is the propellant ignition delay time, and the higher is the burning rate.^{2,3} In order to decrease HTD temperature, metal oxides as catalyst have been widely studied due to their low cost, good thermal stability and catalytic performance.^{4–8} Thus, the

research on the decomposition of AP catalyzed by metal oxides has a great role in the solid propellant industry.

Among the metal oxides, ZnO, as a promising catalyst, is widely used in the chemical industry due to its excellent reactivity, non-toxicity, low cost and thermal stability.⁹ Owing to these advantages, ZnO with different structures such as twin-cones,¹⁰ nanocrystallites,¹¹ nanorod-assembled hollow superstructures¹² and nanotetrapods¹³ have been explored as catalyst to promote the thermal decomposition of AP. However, the underlying catalytic mechanism of ZnO for AP decomposition is still unclear. Especially, the relationship between the catalytic activities and the corresponding structures of ZnO is also not revealed. In our recent work,¹⁴ ZnO nanoplates exhibit a better catalytic activity to promote AP decomposition than ZnO nanorods owing to their large percentage of exposed (001) polar facets, which can not only facilitate the adsorption and diffusion of HClO₄ (a key intermediate product of AP decomposition), but also be favourable for the formation of the active oxygen atoms and further oxidation of NH₃ gas. Due to the large surface energy of exposed (001) facets,^{15–17} ZnO nanoplates will tend to aggregate each other and their good catalytic activity will probably become poor in the mixture of ZnO nanoplates and AP. To overcome this difficulty, the preparation of hierarchical ZnO structures with exposed (001) facets on their external surface should be employed. However, the work has not been reported so far. Therefore, it is of great significance to prepare hierarchical ZnO structures with exposed (001) facets

^a State Key Laboratory of Silicate Materials for Architectures, Wuhan University of Technology, No. 122, Luoshi Road, Wuhan 430070, China. Tel.: +86-27-87669729; Fax: +86-27-87883743. E-mail: tiansq@whut.edu.cn

^b Nanomaterials and Smart Sensors Research Laboratory (NSSRL), State Key Laboratory of Material Processing and Die & Mould Technology, Department of Materials Science and Engineering, Huazhong University of Science and Technology (HUST), No. 1037, Luoyu Road, Wuhan 430074, China. E-mail: dwzeng@mail.hust.edu.cn

^c HuBei Institute of Aerospace Chemotechnology, No. 58, Qinghe Road, Xiangyang 441003, China

† Footnotes relating to the title and/or authors should appear here. Electronic Supplementary Information (ESI) available: [details of any supplementary information available should be included here]. See DOI: 10.1039/x0xx00000x

dominant on their external surface for promoting AP decomposition and reveal the underlying catalytic mechanism.

Herein, hierarchical porous ZnO hollow microspheres with exposed (001) facets on their external surface were prepared by a simple wet chemical method, and their formation mechanism based on the chemical self-transformation was also proposed. In the presence of these ZnO hollow microspheres, the thermal decomposition temperature of AP was lowered from 409 °C to 308 °C with decreased activation energy from 150 ± 14 kJ/mol to 63 ± 7 kJ/mol. This was attributed to the hierarchical porous structures combined with exposed (001) facets dominant on the external surface of microspheres, which can be favourable for the adsorption and reaction of NH_3 and HClO_4 gases from AP. The ZnO dispersed nanorods as a reference were also investigated, and thus the underlying catalytic mechanism related with ZnO microstructures was revealed. Therefore, our work can provide an in-depth insight into the thermal decomposition mechanism of AP as catalyzed by metal oxide micro/nano structures.

Experimental

Sample preparation

All chemicals used in this our work were analytical-grade and were purchased from Shanghai Chemical Reagent Factory of China without further treatment. Distilled water was used in all experiments. In the 50 mL glass beaker, a 0.6585 g (3 mmol) of $\text{Zn}(\text{CH}_3\text{COO})_2 \cdot 2\text{H}_2\text{O}$ was dissolved in 30 mL of glycol under vigorous stirring at room temperature, then ultrasonicated for 10 min, and a transparent solution was obtained. Next, 5 mL of the distilled water was added into the above solution. After being sealed, the beaker was immersed in a 90 °C water bath for 7 h, and then taken out, cooled to the room temperature. The resulting white precipitate was collected by centrifugation and washed with ethanol and distilled water for three times. The washed precipitate was dried in an oven at 80 °C for 8 h and finally was calcined in air at 200 °C for 2 h to remove glycol completely. In order to investigate the controlled synthesis of ZnO hollow microspheres, a series of control experiments were carried out. The time-dependent experiments (0.5 h, 1 h, 1.5 h) were conducted to understand the morphology evolution process. To reveal the function of the distilled water used in the experiment, the prepared solution without the distilled water was used.

Characterization

Powder X-ray diffraction (XRD) patterns were obtained on a PANalytical X'Pert PRO X-ray diffractometer using $\text{Cu K}\alpha 1$ radiation at a scan rate of $0.2^\circ 2\theta \text{S}^{-1}$. The average crystallite size was determined according to the Scherrer equation using the full-width half-maximum data at the diffraction peak of wurtzite (100) plane after correcting the instrumental broadening. Scanning electron microscopy (SEM) was

performed with a FEI Sirion 200 microscope at an accelerating voltage of 20 kV. Transmission electron microscopy (TEM) and HRTEM analysis were conducted using a FEI Tecnai G220 microscope at an accelerating voltage of 200 kV. The Brunauer Emmett Teller (BET) surface area of the powder was analysed by nitrogen adsorption in a Micromeritics ASAP 2020 nitrogen adsorption apparatus (U.S.). The sample was degassed at 180 °C prior to nitrogen adsorption measurements. The BET surface area was determined by a multipoint BET method using the adsorption data in the relative pressure (P/P_0) range of 0.05-0.30. A desorption isotherm was used to determine the pore size distribution by the Barret Joyner Halender (BJH) method, assuming a cylindrical pore model. Average pore size is derived from the combination of BET surface area and pore volume ($4V/A$ by BET). The pore volume refers to BJH adsorption cumulative volume of pores between 1.7 nm and 300 nm diameter.

The catalytic performance toward AP decomposition

The catalytic roles of ZnO hollow microspheres in the thermal decomposition of AP were studied by Diamond TG-DTA thermal analysis instrument (PerkinElmer Instruments) in N_2 atmosphere over the temperature range of 30-500 °C. AP and ZnO hollow microspheres were premixed at a mass ratio of 100:2 to prepare the target sample for thermal decomposition analyses. The activation energies of AP decomposition with and without additives of ZnO hollow microspheres were measured by varying the heating rates. A total sample mass of 2.0 mg was used for all runs.

Results and Discussion

Characterization of ZnO hollow microspheres

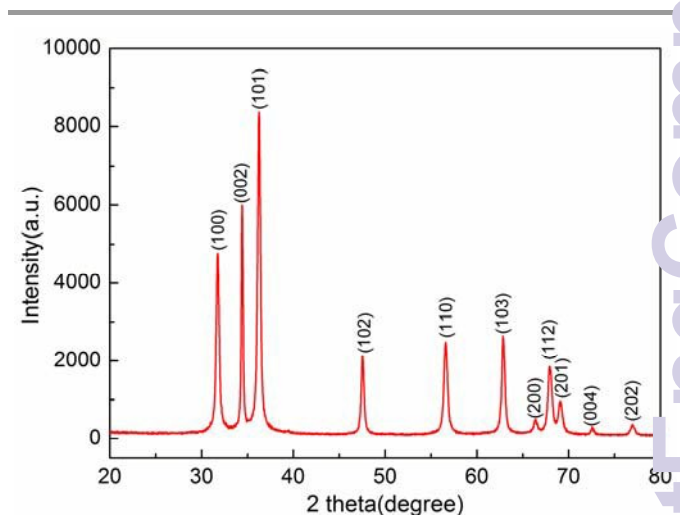


Fig. 1 XRD pattern of ZnO hollow microspheres.

The as-prepared product was characterized by XRD. From the XRD pattern in Fig. 1, all diffraction peaks can be indexed to

wurtzite ZnO (JCPDS card No.36-1451, $a = 0.3249$ nm, $c = 0.5206$ nm). The strong and clear peaks reveal the high purity and crystallinity of the product. No characteristic peaks are observed for other impurities such as $\text{Zn}(\text{OH})_2$. The average crystallite size is about 45 ± 0.5 nm when the (100) diffraction peak is used to evaluate in Scherrer equation. In addition, a larger intensity ratio of (002) diffraction peak to (100) diffraction peak ($I_{(002)}/I_{(100)}$) can be obviously observed after comparing the relative intensities with those from JCPDS card No. 36-1451, usually indicating a larger percentage of exposed (001) polar facet for a single-crystal micro/nano particle.^{9,18} Here, the ZnO hollow microspheres is assembled by many nanorods. Thus, the higher $I_{(002)}/I_{(100)}$ value is caused by the assembly structure with (001) facets of ZnO nanorods exposed dominantly on their external surface, which is in good agreement with the previous reports.^{19,20}

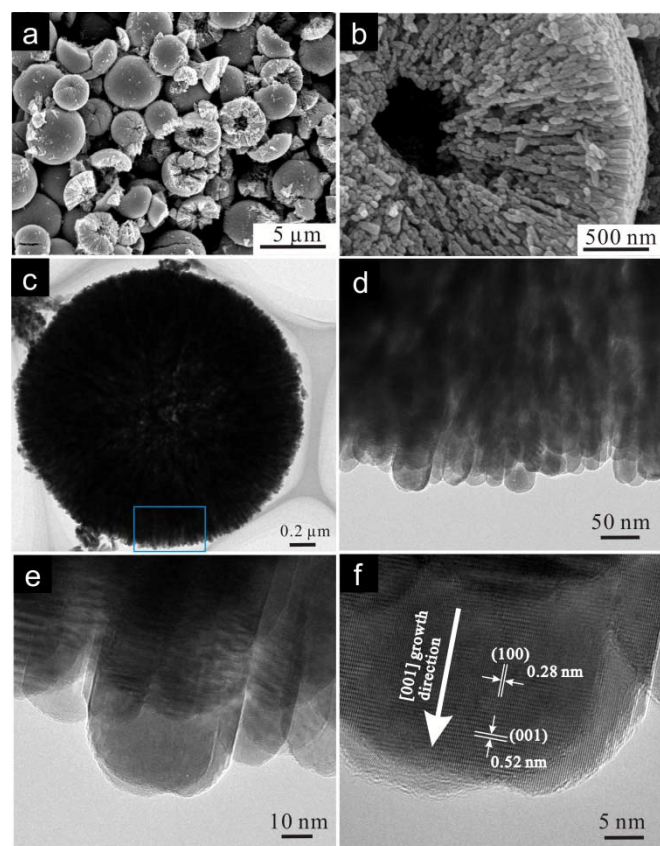


Fig. 2 Characterization of ZnO hollow microspheres: (a) Low- and (b) high- magnification FE-SEM images, (c) TEM image of a single hollow microsphere, (d) Low- and (e) high-magnification TEM images for part of the hollow microsphere, (f) HRTEM image for part of a constituent single nanorod in a hollow microsphere.

Low-magnification FE-SEM observations show that the product is composed of many uniform microspheres with an average diameter of $3 \mu\text{m}$ as shown in Fig. 2a. These microspheres have hollow structures in the central region, suggested by some broken microspheres in Fig. 2b. Although most microspheres are “closed”, further evidence for the

hollow structure can be found from the TEM image. Fig. 2c shows the typical TEM image of a ZnO sphere. Although the shell of the products is too thick to get intensive contrast between the margin and the center, the difference of thickness can be observed between their edge and center, which confirms the formation of well-defined hollow structures. More hollow microspheres can be observed clearly in the TEM image of Fig. S1. In addition, the thickness of the shell for the hollow microspheres is about $0.6 \mu\text{m}$. And the shell is made up of many short nanorods (Fig. 2d and e), which are well aligned and have their growth direction perpendicular to the surface of microspheres. These nanorods exhibit an average diameter of about 40 ± 1.6 nm, which is in good agreement with the above size evaluated by Scherrer equation. The HRTEM image of a single crystalline nanorod in Fig. 2f shows that (001) fringes with a spacing of 0.51 nm run along the nanorod direction while the (100) fringes with a spacing of 0.28 nm are perpendicular to the direction, which is consistent with preferential growth of the nanorod along the c -axis direction (the arrow in Fig. 2f). Besides the bottom of the microspheres, the other parts of the surface on the microspheres were also suffered from HRTEM (shown in Fig. S2) and it can be found that in the selected part, (001) facet of ZnO nanorods is exposed dominantly on the external surface. In this sense, the (001) facets of nanorods are exposed dominantly on the external surface of microspheres, which agrees well with the XRD result. Also, it can be found that many pores are formed in the shells (Figure 2b and c), indicating that the hollow microspheres probably have large surface area.

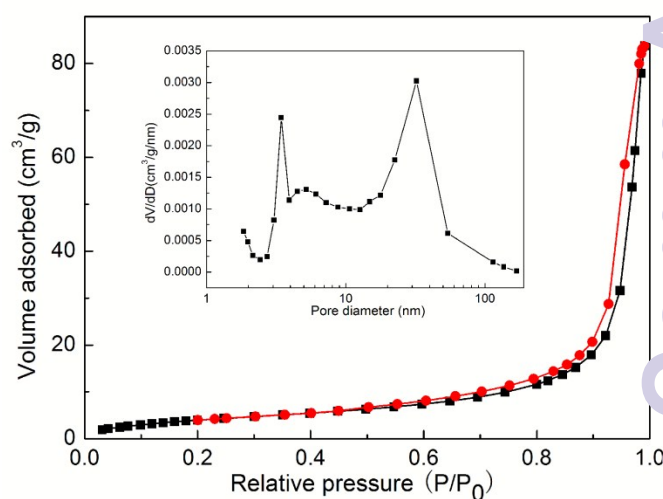


Fig. 3 Nitrogen adsorption-desorption isotherms and pore-size distribution curve (inset) of ZnO hollow microspheres.

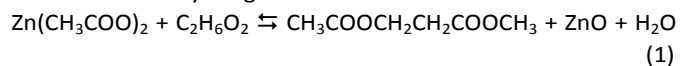
The apparent porous structure of the shell wall was evidenced by the measurement of the Brunauer-Emmett-Teller (BET) surface area and corresponding nitrogen adsorption and desorption isotherms (Fig. 3). The surface area and pore volume of the hollow microspheres are $16.08 \text{ m}^2/\text{g}$ and $0.13 \text{ cm}^3/\text{g}$, respectively. The surface area of $16.08 \text{ m}^2/\text{g}$ is similar to that of other ZnO hollow spheres in the previous

reports,^{21,22} but is relative large compared with other ZnO nanoparticles including flowers, cones and rods.²³ The isotherms are a combination of types I and IV (BDDT classification).²⁴⁻²⁶ At low relative pressures (below 0.2), the isotherms show small adsorption values, indicating the presence of type I micropores. At a high relative pressure range from 0.4 to 1, the curves exhibit two hysteresis loops, implying bimodal pore size distribution in the mesoporous and macroporous regions. In addition, at low relative pressures between 0.45 and 0.90, the hysteresis loop is of type H2, which is related to finer intra-aggregated pores formed between intra-agglomerated primary particles. However, at high relative pressures between 0.9 and 1.0, the hysteresis loop is a typical isotherm of interparticles, which is associated with larger voids produced by the aggregation of single ZnO microspheres, probably indicating the macropores with broad pore size distribution. The bimodal pore-size distribution is further confirmed by the corresponding pore size distributions shown in the inset of Fig. 3. It also can be seen that the hollow microspheres contain micropores (below 2 nm), mesopores (peak pore at ca. 3.5 nm and 32 nm, respectively), and macropores (from 50 nm to 168 nm). These results demonstrate the existence of hierarchically porous structures in the prepared samples on a multilength scale. Such hierarchically organized porous structures might be extremely useful in catalysis as they would provide efficient transport pathways to the interior void space.

The formation mechanism of ZnO hollow microspheres

To develop a comprehensive understanding of the synthesis of ZnO hollow microspheres, it is essential to investigate the influences of some reaction factors. Hence, a variety of reaction parameters such as zinc source, solvent, reaction temperature and reaction time have been investigated.

The investigation of zinc source provides useful information about the formation of ZnO hollow microspheres. Our experimental facts show that $\text{Zn}(\text{CH}_3\text{COO})_2 \cdot 2\text{H}_2\text{O}$ is in favour of the formation of ZnO, but $\text{Zn}(\text{NO}_3)_2 \cdot 6\text{H}_2\text{O}$ is not suitable. Using $\text{Zn}(\text{NO}_3)_2 \cdot 6\text{H}_2\text{O}$ as the precursor, we could not obtain any product. This is because the ZnO nanocrystals can be generated mainly by the esterification between $\text{Zn}(\text{CH}_3\text{COO})_2 \cdot 2\text{H}_2\text{O}$ and glycol,²⁰ expressed in eq 1, when pure glycol is used as solvent or just a small amount of water is added. In the contrast, $\text{Zn}(\text{NO}_3)_2 \cdot 6\text{H}_2\text{O}$ in the solution phase cannot obtain anything.



As a solvent, glycol has been widely used in the preparation of metal oxide nanoparticles due to its high boiling point, great viscosity, strong reducing ability and coordination ability with transition metal ions.²⁷ In the glycol synthesis, the products obtained are generally spherical aggregates of nanoparticles. In our experiments, glycol plays a key role in the formation of hollow structures. ZnO nuclei are generated through the

esterification of $\text{Zn}(\text{CH}_3\text{COO})_2 \cdot 2\text{H}_2\text{O}$ and glycol. These small nuclei have the tendency to aggregate together to decrease the surface energy. Due to great viscosity of glycol, nanocrystals generated in glycol solution will be kinetically very slow so that they can be self-assembled adequately to find a low-energy state and form the twin-microspheres.²⁰ It is worth mentioning that replacing glycol with methanol and keeping other experimental conditions fixed, uniform and short hexagonal ZnO prisms were obtained, as shown in Fig. S3a. These hexagonal prisms are consistent with the crystal structure of wurtzite ZnO. This confirms further that glycol can control the self-assembly of ZnO nanocrystals effectively due to its great viscosity.

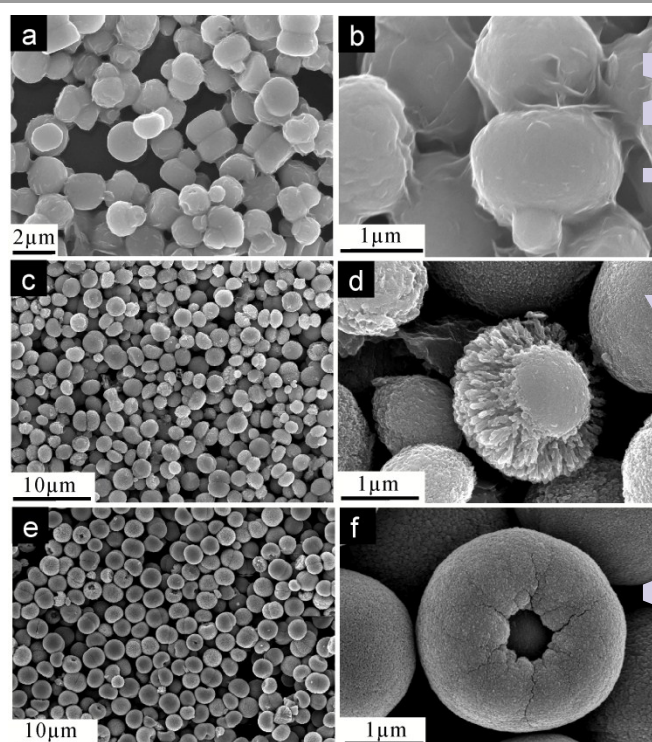
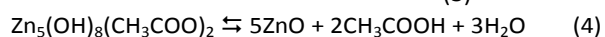
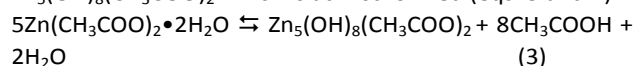


Fig. 4 (a, c, e) Low- and (b, d, f) high-magnification FE-SEM images of the ZnO samples obtained at different reaction times of (a-b) 0.5 h, (c-d) 1 h and (e-f) 1.5 h.

In our experiments, the introduction of water is also critical to form hollow microspheres assembled by nanoparticles. In the glycol solution without water, solid microspheres were obtained and no broken microspheres showed hollow inside as presented in Fig. S3b. A high-magnification SEM image (the upright set of Fig. S3b) reveals that these solid microspheres are made up of nanoparticles, which is in accordance with Shihe Yang's work.²⁸ And the reaction time was extended to 74 h because hydrolysis process of $\text{Zn}(\text{CH}_3\text{COO})_2 \cdot 2\text{H}_2\text{O}$ progressed very slow in the glycol solution without adding water.²⁹ By contrast, with the addition of water, hollow microspheres were completely produced only after 7 h, suggesting that water can promote the hydrolysis process of $\text{Zn}(\text{CH}_3\text{COO})_2 \cdot 2\text{H}_2\text{O}$ to produce ZnO nuclei and CH_3COOH , expressed in eq 2. After these ZnO nuclei are assembled into twin-microspheres, bigger ZnO nanocrystals will grow on the

surface of microspheres and CH_3COOH could selectively dissolve the small nanocrystals with high surface energy in the interior of microspheres. Thus, the hollow microspheres are formed. Our experimental results show that the optimum volume ratio of water to glycol is 1 : 6, only dense particles are obtained for a water/glycol ratio less than 1 : 10 and larger particles are generated at a water/glycol ratio higher than 1 : 4. More detailed investigation is under way.

To further understand the growth mechanism of ZnO hollow microspheres and choose an appropriate reaction time, time-dependent evolution experiments were performed and products collected at different stages are shown in Fig. 4. At the early stage of 0.5 h, the white precipitate is just produced in the solution and exhibits twin-microspheres with an average diameter of 2 μm (Fig. 4a). The XRD patterns of the precipitate in Fig. S4 suggest that the initial product is mainly composed of wurtzite-structure ZnO as well as a few $\text{Zn}_5(\text{OH})_8(\text{CH}_3\text{COO})_2$. Moreover, the intense and sharp reflections indicate that the product is of high purity and crystallinity i.e. no amorphous material exists in the initial product. Therefore, in water-glycol solution, most ZnO nuclei are formed directly by the conversion of $\text{Zn}(\text{CH}_3\text{COO})_2 \cdot 2\text{H}_2\text{O}$ precursor at 90 $^\circ\text{C}$ (eqs. 1 and 2)) and other ZnO nuclei are produced from the hydrolysis of $\text{Zn}_5(\text{OH})_8(\text{CH}_3\text{COO})_2$ which is at first formed (eqs. 3 and 4).



The surfaces of microspheres become very smooth (Fig. 4a and b), which is possibly related to glycol molecules covering on the surface of the product. The presence of glycol molecules in the products is evidenced by the FTIR spectrum in Fig. S5. To observe their detail, the product was annealed at 250 $^\circ\text{C}$ for 2 h to remove glycol completely for characterizations of TEM and FS-SEM. The solid twin-microspheres are further confirmed by the TEM image in Fig. S6a and are composed of many rod-like nanostructures with an average thickness of 50 nm (Fig. S6b). These characterization results indicate that the initial product is mainly composed of twin-microspheres self-assembled by ZnO nanorods through the connection of glycol. Extending the reaction time to 1 h, twin-microspheres are divided into two single microspheres and the diameter is not obviously changed, as shown in Fig. 4c. A close observation in Fig. 4d reveals that the microspheres are assembled by many nanoparticles. The interior of these microspheres is not hollow and consisted of finer nanoparticles. It is noteworthy that no glycol molecules are adsorbed on the surface of the product. With further increasing the reaction time up to 1.5 h, an opening part appears on the most microspheres (Fig. 4e) and hollow space in the central region is produced as seen from higher-magnification image of Fig. 4f. When the reaction time is prolonged to 7 h, ZnO hollow microspheres with high porous surfaces are obtained. As the reaction time increases further, there is unnoticeable change on the morphologies of the ZnO products.

On the basis of morphology of the intermediate product in the time-dependent evolution process, the formation

mechanism of ZnO hollow microspheres is proposed. The whole formation process included two stages: the formation of twin-microspheres self-assembled by ZnO nanocrystals, the chemical self-transformation from the tiny ZnO nanocrystals in the linking part and interior core to nanorods with a larger size in the external shell, creating the hollow interior space, as shown schematically in Fig. 5. In the initial stage, ZnO nuclei can be generated by the esterification of $\text{Zn}(\text{CH}_3\text{COO})_2 \cdot 2\text{H}_2\text{O}$ and glycol, and the hydrolysis process of $\text{Zn}(\text{CH}_3\text{COO})_2 \cdot 2\text{H}_2\text{O}$ in water/glycol solution. Due to the high boiling point and great viscosity of glycol/water solution,^{20,28} these ZnO nuclei will grow up and then move kinetically very slow so that they can be self-assembled adequately to find a low-energy state and form the twin-microspheres.³⁰ The linking part of twin spheres has high surface area and can be dissolved easily by CH_3COOH , which is produced from eq. 2 (The reaction is dynamic and thus leads to dissolution-recrystallization process). The nanocrystals located on other outer surfaces would serve as starting points for the subsequent crystallization process. During the ripening process, epitaxial growth from the initial nanocrystals along the [001] direction is dominant due to the one-dimensional growth habit of the hexagonal ZnO crystal.^{20,28,29,31} As a result, ZnO nanorods would grow on the other outer surfaces at the expense of the linking part. Probably, before the twin spheres were completely divided into two semispheres, the formation of some ZnO nanorods occurs on the outer surfaces of twin spheres (Fig. S6). Then, the twin spheres are divided into two ZnO semispheres with some nanorods on the most part of outer surface and a few nanocrystals on the other parts (Fig. 4d). Subsequently, the nanocrystals in the inner core of ZnO semispheres have high surface area due to their small size and can be dissolved easily.²⁰ The nanocrystals and nanorods located on other outer surfaces would serve as starting points for the subsequent crystallization process. The small nanocrystals in the core would provide the source for the durative growth along [001] of nanorods in the shell during the solid evacuation. When the reaction time is extended, the size of the core is reduced gradually while the hollow volume is enlarged. Finally, the nanorod-assembled hollow spheres are obtained with complete depletion of the core with a longer reaction time of 7 h. In this sense, the chemical self-transformation can be explained for this hollowing process.

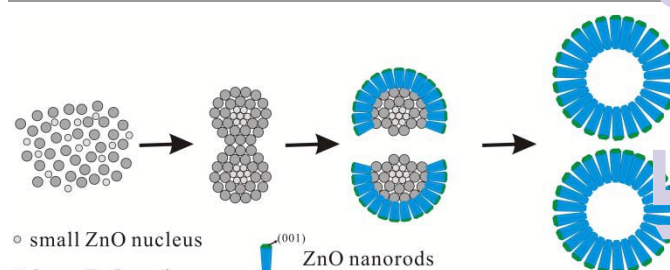


Fig. 5 Schematic illustration for the formation process of ZnO hollow microspheres.

The Catalytic Activity for AP Decomposition

Based on the above results, the as-prepared ZnO hollow microspheres exhibit exposed (001) facets of nanorods dominant on their external surface, hierarchical porous structures and large surface area. Due to these advantages, ZnO hollow microspheres were explored as an additive in promotion of the thermal decomposition of AP. Fig. 6 shows the raw DTA data for pure AP and mixture of AP with the as-prepared ZnO particles. For pure AP, the thermal decomposition proceeds in two steps are clearly indicated in the DTA curves. The first step starts at about 290 °C (it can be seen clearly in the TG curve of Fig. S7) and shows a peak at 312 °C, which is named as the low-temperature decomposition (LTD). The LTD is a heterogeneous process beginning with proton transfer in the AP subsurface, yielding NH_3 and HClO_4 adsorbed in the porous structure that forms during the reaction, followed by the decomposition of HClO_4 and reaction with NH_3 . As the LTD proceeds, NH_3 accumulates on the surface suppressing the reversible proton-transfer process and then the reaction ceases on an NH_3 -covered surface.⁶ The second step starts at about 350 °C (shown in Fig. S7), showing a peak at 409 °C in the DTA curve, which is assigned to the high-temperature decomposition (HTD).⁵ The HTD involves the simultaneous dissociation and sublimation of AP to $\text{HClO}_4(\text{g})$ and $\text{NH}_3(\text{g})$. The total process can be expressed as follows:^{6,10}

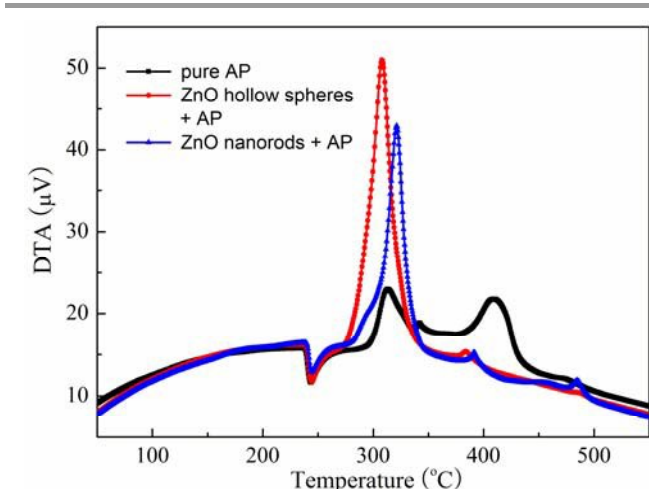
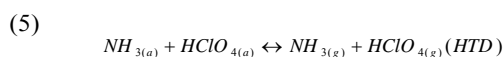


Fig. 6 DTA curves of pure AP and mixtures of AP with the as-prepared ZnO particles at a heating rate of 20 K/min.

For the present work, it is interesting that the HTD process is accelerated when AP is mixed with our as-prepared ZnO particles. With ZnO hollow microspheres, the HTD process of AP disappears completely to show a sole exothermic process in the temperature range from 260 °C to 360 °C (shown in Fig. S7), in which AP is catalyzed to decompose at a temperature as low as 308 °C and release the decomposition heat as much as 1174 J/g. By contrast, in the presence of ZnO dispersed nanorods as a comparison, the HTD process of AP does not

disappear completely, but the decomposition heat of AP is increased from 417 J/g to 959 J/g, and the maximum decomposition temperature is reduced from 409 °C to 321 °C, respectively. As can be seen, ZnO hollow microspheres assembled by nanorods exhibit a better catalytic effect for AP decomposition than dispersed nanorods.

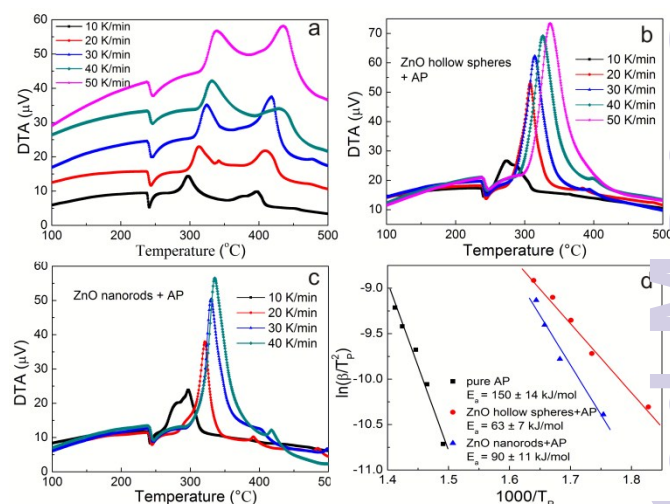


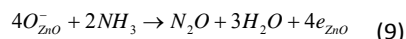
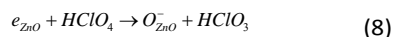
Fig. 7 DTA curves of (a) pure AP and (b-c) AP with the as-prepared ZnO samples at the given heating rates, and (d) Dependence of $\ln(\beta/T_p)$ on $1/T_p$ for AP decomposition, scatter points are experimental data and lines denote the linear fitting results.

To further study the catalytic role of the as-prepared ZnO particles toward AP decomposition, kinetic parameters for AP decomposition with ZnO particles are calculated from the exothermic peak temperature dependence as a function of heating rate. Fig. 7a-c shows the DTA curves of pure AP, the mixtures of AP with ZnO hollow microspheres and nanorods at different heating rates. It can be seen that the decomposition temperature of AP is dependent on the heating rate with or without ZnO particles. The relationship between decomposition temperature and heating rate can be described by Kissinger correlation (eq. 5)^{5,13,14}

$$\ln\left(\frac{\beta}{T_p^2}\right) = \ln\left(\frac{AR}{E_a}\right) - \frac{E_a}{RT_p} \quad (7)$$

Where β is the heating rate in degrees Celsius per minute, T_p is the peak temperature, R is the ideal gas constant, E_a is the activation energy, and A is the pre-exponential factor. According to the eq 7, the term $\ln(\beta/T_p^2)$ varies linear with $1/T_p$, yielding the kinetic parameters of activation energy from the slope of the straight line. Fig. 7d shows the experimentally measured $\ln(\beta/T_p^2)$ versus $1/T_p$ with and without ZnO particles. For pure AP, the activation energy of HTD is calculated to be 150 ± 14 kJ/mol, which is close to the value previously reported in literature.^{13,32} In the presence of ZnO hollow microspheres and dispersed nanorods, the activation energy of AP decomposition is decreased to 63 ± 7 kJ/mol and 90 ± 11 kJ/mol, respectively. On the basis of the above data, the two

kinds of ZnO particles show good catalytic activity towards AP decomposition. This is related to the negative oxygen ions O^- produced from the electron transfer between ZnO and $HClO_4(a)$, which may reduce the concentration of NH_3 partially.^{2,33} Since $HClO_4(a)$ adsorbs on the surface of ZnO particles and forms negative oxygen ions O^- by combining with intrinsic electrons from ZnO above 250 °C. These negative oxygen ions formed in eq 8 might react with NH_3 to produce N_2O and H_2O expressed as the eq 9 so that the concentration of $NH_3(a)$ was decreased.



Therefore, AP decomposition is accelerated with the addition of ZnO particles. In addition, ZnO hollow microspheres exhibit better catalytic activities for AP decomposition than the dispersed ZnO nanorods, which is probably attributed to their different structures including the surface area, crystallinity and exposed facets. In the surface area, ZnO hollow microspheres and dispersed nanorods exhibit 16.08 m^2/g and 4.12 m^2/g (obtained from BET measurement), respectively. In this sense, the hierarchical microspheres exhibit larger surface area than the dispersed nanorods which can be easily agglomerated. Usually, the sample with larger surface area can provide more active sites for the adsorption and diffusion of $HClO_4$ and NH_3 gases, leading to a better catalytic activity. Thus, the hierarchical hollow microspheres perform better catalytic activity than the dispersed nanorods. In the crystallinity, the diffraction peaks in the XRD patterns of the two kinds of ZnO samples are very sharp (Fig. 1 and Fig. S8), implying the high crystalline of two ZnO samples. In the exposed facets, the hollow microspheres exhibit the (001) facets of ZnO crystal dominant exposed on their external surface, while the external surface of ZnO nanorods are enclosed by (001) facets, {101} and {100} facets as shown in the SEM and TEM images of Fig. S9. According to the density functional theory calculation and experiment result in the our previous report,¹⁴ the exposed (001) facet are more favourable for the adsorption of $HClO_4$ and NH_3 gases than other facets due to its higher surface energy and charge interaction, while the {100} facets are not. Moreover, the (001) facet can facilitate the formation of active oxygen from the adsorbed $HClO_4$ which can lead to the oxidation reaction of NH_3 gas more completely in the catalytic decomposition of AP. For dispersed ZnO nanorods, their {100} facets, {101} facets and (001) facets are all exposed to the $HClO_4$ and NH_3 gases, and can adsorb these gases competitively as shown in Fig. 8a. A large part of the gases can be adsorbed on the {100} facets but not be decomposed.¹⁴ This will influence the catalytic properties of ZnO nanorods in promoting AP decomposition. For the assembly structure with (001) facets exposed on the external surface, most of the $HClO_4$ and NH_3 gases will probably at first be absorbed on the (001) facets and can be decomposed. In this sense, ZnO hollow microspheres with the exposed (001) facets on their external surface will adsorb more $HClO_4$ and NH_3 gases, and produce more active oxygen,

promoting the continuous and complete decomposition of AP on the (001) facets and in the hollow section, as shown in Fig. 8b. Therefore, the ZnO hierarchical hollow microspheres with larger surface area and the exposed (001) facets dominant on their external surface exhibit better catalytic performance for AP decomposition than the dispersed nanorods. Furthermore, these hierarchical structures show a good stability than the nanorods during high temperature stage of AP decomposition.

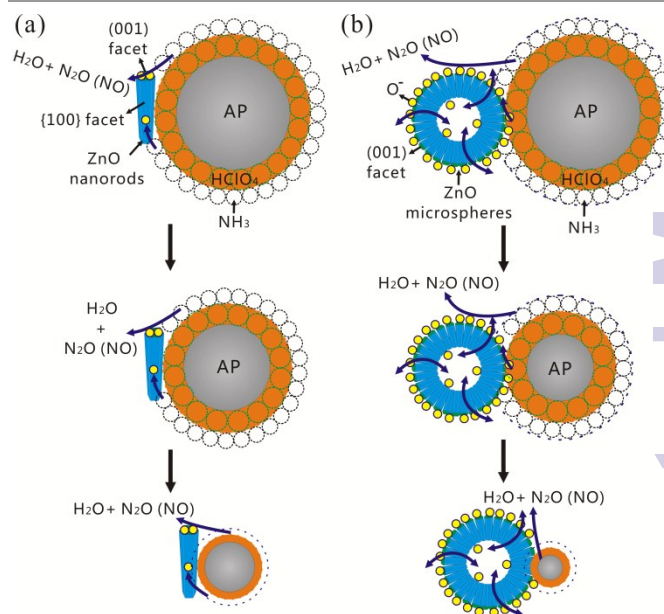


Fig. 8 Schematic illustration for the decomposition process of AP catalyzed by (a) ZnO dispersed nanorods and (b) ZnO hollow microspheres.

Conclusions

Hierarchical porous ZnO hollow microspheres were successfully obtained by a simple one-pot wet chemical method using zinc acetate as a precursor in the glycol/water solution at low temperature, and they showed a good catalytic effect on the thermal decomposition of AP. The presence of ZnO hollow microspheres significantly reduces the activation energy of AP decomposition from 150 ± 14 kJ/mol to 63 ± 7 kJ/mol and lowers the decomposition temperature from 409 °C to 308 °C compared with pure AP. This is mainly attributed to the hierarchical porous structures and the active (001) facets dominant exposed on the external surface for the adsorption of $HClO_4$ and NH_3 gases, which is further confirmed by the control experiment dispersed nanorods used as catalyst to promote AP decomposition. The decomposition mechanism of AP catalyzed by ZnO hierarchical structures dependent on the exposed facets on the external surface is also revealed and thus ZnO hollow microspheres will be a promising catalyst used in the AP-based propellant.

Acknowledgements

This work was supported by the National Natural Science Foundation of China (Grant Nos. 51402225, 51572075 and 51461135004), Doctoral Fund of Ministry of Education Priority Development Projects (No. 20130143130002), Hubei Provincial Natural Science Foundation (No. 2014CFB867), the Fundamental Research Funds for the Central Universities (WUT: 2014-IV-012) and the China Postdoctoral Science Foundation (No. 2014M552097 and 2015T80846). We also thank the Analytic Testing Center of HUST for the help with carrying out XRD, TEM, FESEM, TG/DTA and FTIR analysis.

Notes and references

- V. V. Boldyrev, *Thermochim. Acta*, 2006, **443**, 1-36.
- N. Li, M. H. Cao, Q. Y. Wu and C. W. Hu, *CrystEngComm*, 2012, **14**, 428-434.
- H. Xu, X. B. Wang and L. Z. Zhang, *Powder Technol.*, 2008, **185**, 176-180.
- L. N. Jin, Q. Liu and W. Y. Sun, *CrystEngComm*, 2012, **14**, 7721-7726.
- L. P. Li, X. F. Sun, X. Q. Qiu, J. X. Xu and G. S. Li, *Inorg. Chem.*, 2008, **47**, 8839-8846.
- D. L. Reid, A. E. Russo, R. V. Carro, M. A. Stephens, A. R. LePage, T. C. Spalding, E. L. Petersen and S. Seal, *Nano Lett.*, 2007, **7**, 2157-2161.
- Y. P. Wang, J. W. Zhu, X. J. Yang, L. D. Lu and X. Wang, *Thermochim. Acta*, 2005, **437**, 106-109.
- Z. X. Zhou, S. Q. Tian, D. W. Zeng, G. Tang and C. S. Xie, *J. Alloy Compd.*, 2012, **513**, 213-219.
- A. McLaren, T. Valdes-Solis, G. Q. Li and S. C. Tsang, *J. Am. Chem. Soc.*, 2009, **131**, 12540-12541.
- X. F. Sun, X. Q. Qiu, L. P. Li and G. S. Li, *Inorg. Chem.*, 2008, **47**, 4146-4152.
- M. Zheng, Z. S. Wang, J. Q. Wu and Q. Wang, *J. Nanopart. Res.*, 2010, **12**, 2211-2219.
- J. Z. Yin, Q. Y. Lu, Z. N. Yu, J. J. Wang, H. Pang and F. Gao, *Cryst. Growth Des.*, 2010, **10**, 40-43.
- G. Tang, Y. W. Wen, A. M. Pang, D. W. Zeng, Y. G. Zhang, S. Q. Tian, B. Shan and C. S. Xie, *CrystEngComm*, 2013, **16**, 570-574.
- G. Tang, S. Q. Tian, Z. Z. Zhou, Y. W. Wen, A. M. Pang, Y. G. Zhang, D. W. Zeng, H. T. Li, B. Shan and C. S. Xie, *J. Phys. Chem. C*, 2014, **118**, 11833-11841.
- X. G. Han, H. Z. He, Q. Kuang, X. Zhou, X. H. Zhang, T. Xu, Z. X. Xie and L. S. Zheng, *J. Phys. Chem. C*, 2009, **113**, 584-589.
- E. S. Jang, J. H. Won, S. J. Hwang and J. H. Choy, *Adv. Mater.*, 2006, **18**, 3309-3312.
- S. Q. Tian, F. Yang, D. W. Zeng, C. S. Xie, *J. Phys. Chem. C*, 2012, **116**, 10586-10591.
- G. R. Li, T. Hu, G. L. Pan, T. Y. Yan, X. P. Gao and H. Y. Zhu, *J. Phys. Chem. C*, 2008, **112**, 11859-11864.
- S. Y. Gao, H. J. Zhang, X. M. Wang, R. P. Deng, D. H. Sun and G. L. Zheng, *J. Phys. Chem. B*, 2006, **110**, 15847-15852.
- P. Hu, X. Zhang, N. Han, W. C. Xiang, Y. B. Cao and F. L. Yuan, *Cryst. Growth Des.*, 2011, **11**, 1520-1526.
- J. Zhang, S. R. Wang, Y. Wang, M. J. Xu, H. J. Xia, S. M. Zhang, W. P. Huang, X. Z. Guo and S. H. Wu, *Sens. Actuators, B*, 2009, **139**, 411-417.
- J. G. Yu and X. X. Yu, *Environ. Sci. Technol.*, 2008, **42**, 4902-4907.
- L. P. Xu, Y. L. Hu, C. Pelligra, C. H. Chen, L. Jin, H. Huang, S. Sithambaram, M. Aindow, R. Joesten and S. L. Suib, *Chem. Mater.*, 2009, **21**, 2875-2885.
- J. G. Yu, W. Liu and H. G. Yu, *Cryst. Growth Des.*, 2008, **8**, 930-934.
- J. G. Yu, J. Zhang and S. W. Liu, *J. Phys. Chem. C*, 2010, **114**, 13642-13649.
- K. S. W. Sing, D. H. Everett, R. A. W. Haul, L. Moscou, R. A. Pierotti, J. Rouquerol and T. Siemieniewska, *Pure & Appl. Chem.*, 1985, **57**, 603-619.
- H. Deng, X. L. Li, Q. Peng, X. Wang, J. P. Chen and Y. D. Li, *Angew. Chem., Int. Ed.*, 2005, **117**, 2842-2845.
- Y. C. Qiu, W. Chen, S. H. Yang, B. Zhang, X. X. Zhang, Y. C. Zhong and K. S. Wong, *Cryst. Growth Des.*, 2010, **10**, 177-183.
- H. H. Wang, C. S. Xie and D. W. Zeng, *J. Cryst. Growth*, 2005, **277**, 372-377.
- F. Li, F. L. Gong, Y. H. Xiao, A. Q. Zhang, J. H. Zhao, S. M. Fang and D. Z. Jia, *ACS Nano*, 2013, **7**, 10482-10491.
- M. Mo, J. C. Yu, L. Zhang and S. K. A. Li, *Adv. Mater.*, 2005, **17**, 756-760.
- J. C. Oxley, J. L. Smith and B. R. Valenzuela, *J. Energy Mater.*, 1995, **13**, 57-91.
- A. A. Said, *J. Thermal Anal.*, 1991, **37**, 959-967.